LETTERS

Simultaneous teleseismic and geodetic observations of the stick–slip motion of an Antarctic ice stream

Douglas A. Wiens[1], Sridhar Anandakrishnan[2], J. Paul Winberry[2] & Matt A. King[3]

Long-period seismic sources associated with glacier motion have been recently discovered[1,2], and an increase in ice flow over the past decade has been suggested on the basis of secular changes in such measurements[3]. Their significance, however, remains uncertain, as a relationship to ice flow has not been confirmed by direct observation. Here we combine long-period surface-wave observations with simultaneous Global Positioning System measurements of ice displacement to study the tidally modulated stick–slip motion of the Whillans Ice Stream in West Antarctica[4,5]. The seismic origin time corresponds to slip nucleation at a region of the bed of the Whillans Ice Stream that is likely stronger than in surrounding regions and, thus, acts like an 'asperity' in traditional fault models. In addition to the initial pulse, two seismic arrivals occurring 10–23 minutes later represent stopping phases as the slip terminates at the ice stream edge and the grounding line. Seismic amplitude and average rupture velocity are correlated with tidal amplitude for the different slip events during the spring-to-neap tidal cycle. Although the total seismic moment calculated from ice rigidity, slip displacement, and rupture area is equivalent to an earthquake of moment magnitude seven (M_w 7), seismic amplitudes are modest (M_s 3.6–4.2), owing to the source duration of 20–30 minutes. Seismic radiation from ice movement is proportional to the derivative of the moment rate function at periods of 25–100 seconds and very long-period radiation is not detected, owing to the source geometry. Long-period seismic waves are thus useful for detecting and studying sudden ice movements but are insensitive to the total amount of slip.

The mass balance of continental ice sheets is in large part controlled by the flow rates of ice streams and outlet glaciers. The dynamics of ice flow, and in particular the influence of basal properties, has received considerable attention in recent years because of concern about possible rapid future rises in sea level due to the acceleration of these ice streams[6–8]. Numerical models of ice flow include sliding and basal deformation physics; however, they are incapable of explaining the recent observations which suggest that some motion may occur through stick–slip sliding, similar to that which occurs in earthquake faults[9]. Outlet glaciers in Greenland and several other locations produce globally recorded long-period seismic waves[1]. It has been suggested that these events result from sudden glacier motion with a timescale of about 50 s (ref. 2), and that the increasing frequency of these events in recent years may be related to climate change[3]. However, the mechanics and interpretation of these 'glacial earthquakes' remain highly uncertain, as no simultaneous observations have been published from the source regions.

Global Positioning System (GPS) observations show that the ice plain of the Whillans Ice Stream (WIS, formerly Ice Stream B) in West Antarctica undergoes tidally modulated stick–slip motion twice per day[4,5]. During each slip event, the ice plain of the WIS (which is greater than 200 km × 100 km in area and approximately 600 m thick) moves by up to 70 cm in approximately 25 min. The expression for the seismic moment of an elastic dislocation[10], $M_0 = \mu DA$, where μ is the rigidity of glacial ice (3.5×10^9 N m^{-1}), D is the dislocation and A is the slip area, shows that this event is equivalent to a M_w-7.0 earthquake. However, because of the slow average rupture velocity (~150 m s^{-1}) and long slip time at a given location, its source duration is nearly two orders of magnitude longer than that of a similarly sized tectonic earthquake. In the years 2001–2003, a deployment of 43 broadband seismographs in the Trans-Antarctic Mountains and East Antarctic interior (approximately 1000 km from the WIS) detected Rayleigh waves originating from the WIS that correlated with the expected times of tidally triggered slip[11].

Simultaneous seismic and geodetic observations made during 2004 allow us to determine the mechanism for glacial generation of seismic waves and to better constrain the slip characteristics of the WIS. An array of 19 GPS instruments (see Supplementary Table 1) operating at a sampling rate of 0.1 Hz was deployed on the WIS to record the ice stream motion as part of the Tidal Modulation of Ice-Stream Flow (TIDES) project[12]. The ice stream slip events were also well recorded at the borehole Global Seismic Network stations near the South Pole (station QSPA; 89.928° S, 145.0° E) and in the McMurdo Dry Valleys (station VNDA; 77.517° S, 161.853° E) at distances of 620 and 990 km from the WIS, respectively (Fig. 1, upper inset).

Examination of the GPS records from the WIS (see Methods) shows that ice stream slips repeatedly originate near the same location on the ice plain (Fig. 1). Rupture propagation is about 500–1,000 m s^{-1} within 20–30 km of the nucleation point, but becomes much slower (~100 m s^{-1}) in more distant regions of the ice stream. Slip magnitude becomes smaller progressively farther upstream of the nucleation point; however, the slip retains significant amplitude down to the grounding line and onto the Ross Ice Shelf. The slips terminate near the grounding line to the northwest of the nucleation point about 20–30 min after initiation. The slips are tidally modulated; one slip episode occurs around the time of the high ocean tide and a second occurs 5–12 h later, with the intervals converging to 12 h during times of low tidal amplitude (neap tide). In contradiction to initial reports[5], the amount of slip is proportional to the inter-event time and, thus, to the stress accumulated since the last slip event. Times of the slip episodes are given in Supplementary Table 2.

Seismic Love waves are recorded at VNDA and QSPA, and Rayleigh waves at VNDA; Rayleigh waves are not well recorded at QSPA, owing to the source radiation pattern. Seismogram signals are detectable at periods of 20–150 s and typically show three arrivals over a time span of 12–23 min (Fig. 2b). Because the recorded seismic periods are much shorter than the rupture duration, the signal is highly band limited, and the observed seismic radiation should

[1]Department of Earth and Planetary Sciences, Washington University, St Louis, Missouri 63130, USA. [2]Department of Geosciences, The Pennsylvania State University, University Park, Pennsylvania 16802, USA. [3]School of Civil Engineering and Geosciences, Newcastle University, Newcastle upon Tyne NE1 7RU, UK.

correspond to rapid changes in the seismic moment rate. The onset of the first seismic arrival, when corrected for surface-wave propagation between source and receiver, occurs 20–150 s after the first onset of slip at the GPS station closest to the inferred rupture source. Thus, the initial seismic pulse records the rapid increase in moment rate resulting from the initial fast expansion of the rupture.

The seismic waveforms show systematic variations as a function of the tidal cycle, with larger delays between the first and third arrivals for smaller Ross Sea ocean tidal amplitudes (Fig. 3a). The GPS observations suggest that the average rupture velocity is correlated with the tidal amplitude (Fig. 3b). This suggests that the second and third seismic pulses probably radiate from specific spatial regions within the rupture zone, and that their timing is determined by their distances from the rupture origin and the rupture velocity. Differences in the timing of the second and third arrivals relative to the first indicate that they do not originate from the rupture onset location.

We implement a simple grid-search procedure to find the source location that best fits both the seismic arrival times and the average

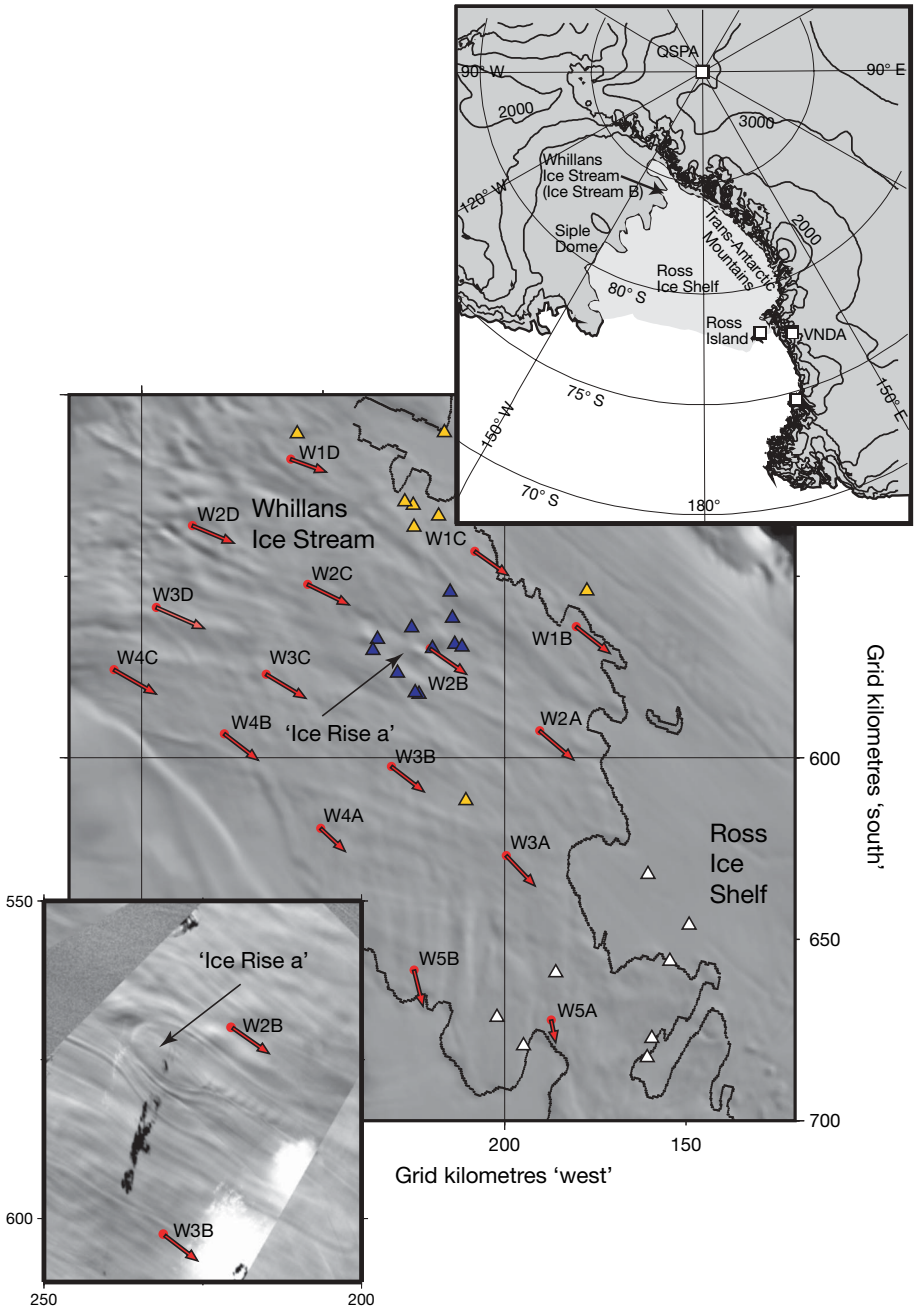

Figure 1 | The Whillans Ice Stream, the positions of the sensors and the positions of the slip nucleation and seismic source locations. TIDES GPS receivers (red circles), the slip nucleation points determined from GPS (blue triangles) and the approximate source regions for the second (orange triangles) and third (white triangles) seismic surface-wave arrivals, calculated from the seismic arrival times and the average rupture velocity for nine slip events from 16–20 November 2004 are shown on a Moderate Resolution Imaging Spectroradiometer mosaic map. The grounding line is marked with a black line[24]. Red arrows indicate the direction of ice flow determined from GPS, with arrow length proportional to speed (for scale, the red arrow at W2B represents 392.4 m yr $^{-1}$). Coordinates are given in a grid system with the origin at the South Pole, the 'south' axis oriented along longitude 180°, and the 'west' axis along longitude 90° W. The upper inset shows the location of the Whillans Ice Stream and the QSPA and VNDA seismic stations, among other permanent seismic stations (open squares). Contours indicate surface elevation in meters. The lower inset, which has the same axes as the main panel, is an enlarged SPOT image showing ice flow features in the region of the rupture nucleation points and 'Ice Rise a'[3], which is thought to represent a region of reduced subglacial water and higher basal friction.

rupture velocity as determined from the GPS observations (see Methods). The source regions of the second seismic arrivals are preferentially located along the southern lateral edge of the ice stream, suggesting that each of the second pulses may result from a rapid decrease in the moment rate when the rupture front reaches that edge. The source regions of the third seismic arrivals are clustered near the grounding line about 100 km northwest of the nucleation point. The origin times calculated from the third seismic arrivals at VNDA and QSPA correspond closely to the arrival times of the peak rupture velocity at GPS receiver W5B (Fig. 1) near the grounding line in this region. This suggests that each third (and final) arrival represents a 'stopping phase' in which the moment rate function begins to decrease owing to the decrease in slip area after the slip reaches the grounding line.

The slip repeatedly nucleates in the same region, near GPS receiver W2B (Fig. 1). The uncertainty in the nucleation point locations is similar to the scatter of the locations, so it is not clear whether or not all the events nucleate at the same point. This site has been previously identified as 'ice rise a' (although the feature is not an ice rise, we continue to refer to it as such)[13], a patch of higher friction on the ice stream bed inferred on the basis of flow lines and slightly increased ice elevations[14]. This region is readily visible in the SPOT (Satellite Pour l'Observation de la Terre) image (Fig. 1, lower inset) and also defines an area of low effective reflection coefficient on radar images[15], which is commonly interpreted as indicating an absence of subglacial water. This suggests that the stick–slip characteristics of the WIS are controlled by an area of higher friction that resembles a classic barrier or asperity found in earthquake fault models[16,17]. Thus, a simple explanation consistent with the data is that the WIS motion is affected by both the tidal modulation and by this patch of greater friction, perhaps because of bed composition or hydrological conditions. Resistance at the asperity results in little motion of the ice downstream of the asperity except when loading exceeds the breaking point and a slip event occurs, unlike in the neighbouring Bindschadler Ice Stream, which displays tidally modulated velocities without any slip events[18].

The transverse component of the seismogram at QSPA and the vertical component at VNDA have good signal-to-noise ratios in the 0.012–0.04-Hz frequency band. Although these band-limited data are not sufficient to construct a well-constrained inverse solution, we can obtain significant insight from forward modelling. We model the first packet of surface waves assuming there to be a double-couple source at a shallow depth (1 km); the two later packets are more complicated and variable, probably as a result of the interference of stopping phases from different parts of the slip region.

The modelling shows that, as expected, the seismograms are only sensitive to the spectral components of the moment rate function within the 0.012–0.04-Hz band; the absence of any additional packets

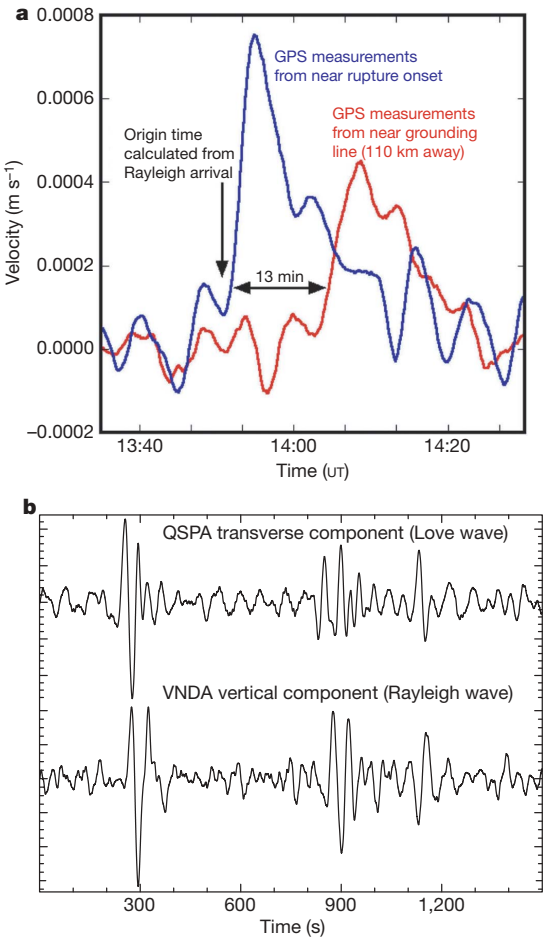

Figure 2 | GPS and seismic records of Whillans slip events. a, Ice velocity computed from GPS data recorded near the slip nucleation point (W2B) and near the grounding line (W5A). See Methods for processing details. **b**, Typical seismograms of Whillans slip events recorded at VNDA and QSPA, showing the three main surface-wave packets.

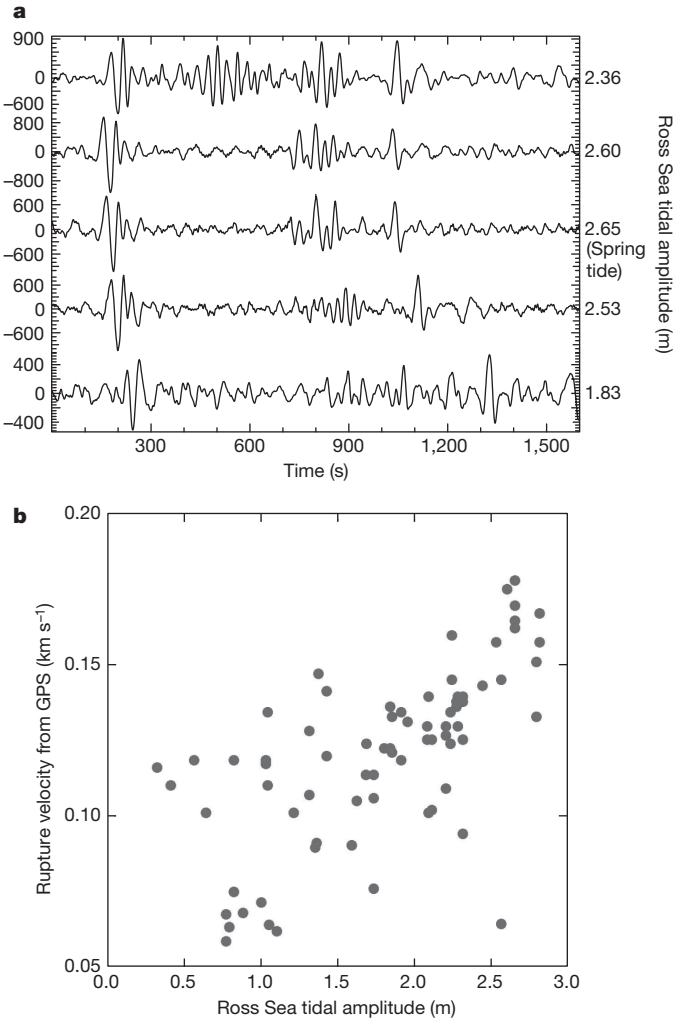

Figure 3 | The effect of Ross Sea tidal amplitude on seismograms and the average rupture velocity from GPS. a, Seismograms showing the effects of the tidal cycle on the seismic waveforms (specifically the QSPA transverse component, 25–100 s passband). Rupture velocity correlates with tidal amplitude, resulting in shorter durations for high tides. Tidal amplitude in metres is calculated using model CATS02.01 (ref. 25), and seismogram amplitude is shown in digital counts. **b**, Average rupture velocity determined by GPS as a function of tidal amplitude.

within the first 400 s suggests that the moment rate function is extremely smooth during the rupture expansion phase. In a simple elastic dislocation model, the source time function is the slip area as a function of time convolved with the slip function at any given point along the dislocation. The duration of slip at most GPS sites and the rupture propagation time are both about 700 s, suggesting that the total duration of the time function is approximately 1,400 s. We achieve a good fit to the initial waveforms using an offset inverse cosine function with a period of 800–1,400 s (Fig. 4). The relative amplitudes of the Love and Rayleigh waves at QSPA and VNDA are well fit by a rupture on a plane dipping very shallowly to the west-northwest (strike, 210°; dip, 3°), consistent with the ice stream motion direction. The observed surface-wave pulse is radiated by the initial part of this function, which has the highest spectral amplitude within the frequency band with good signal.

Because the seismic amplitudes within the passband are controlled by the high-frequency characteristics of the moment rate function rather than its overall amplitude, the total seismic moment of the event, and thus the slip area and amplitude, cannot be constrained by seismic observations alone. The seismic amplitudes are instead a function of the rapidity of the rupture, which is correlated with tidal amplitude, rather than the slip displacement or area. Owing to the extremely long source duration, the seismic amplitudes at periods of 25–100 s are much smaller than would be expected for a tectonic earthquake with this total slip and the assumed elastic properties ($M_w \approx 7.0$). We estimate that the seismic amplitudes correspond to surface wave magnitudes of M_s 3.6 to M_s 4.2, using the method of Russell[19] and extending the period to 50 s. The events are also probably invisible at normal mode periods (200–3,000 s), as several studies searching for undetected sources in this band have failed to find them[20,21]. This is probably due to the degenerate nature of horizontal dislocations very near the Earth's surface, which causes seismic excitation to go to zero at ultralong periods[22], and to the high ambient noise level in this band[23].

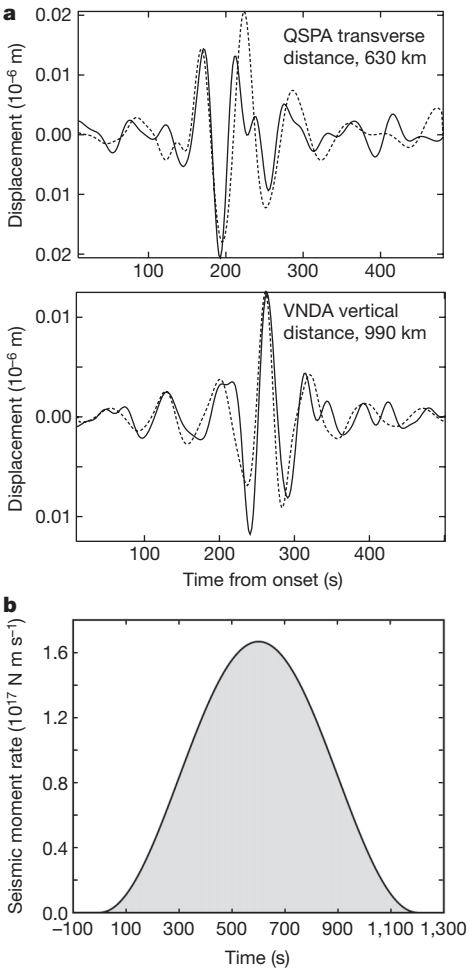

Figure 4 | Modelling the initial seismic signals of the slip events. **a**, Observed seismograms (solid lines) of the first Love wave packet (QSPA, upper graph) and Rayleigh wave packet (VNDA, lower graph) for the 0.012–0.04 Hz passband, along with synthetic seismograms (dashed lines) calculated for a dip–slip elastic dislocation dipping 3° towards N60°W at a depth of 1 km. **b**, Seismic moment rate function used to calculate synthetics in **a**. The total moment release and long-period characteristics of the moment rate function are not well determined, because they are outside the passband of the signal. We note that the later parts of the function involving a decrease in the moment rate are too late to affect the initial waveforms modelled in **a**.

The observation of teleseismic surface-wave radiation from the WIS slip events has a number of wider implications. Ekstrom *et al.*[1] discovered long-period seismic sources co-located with glaciers in Greenland and Alaska and at Totten Glacier in Antarctica, using global seismic data, and concluded that they represent glacial slip events. Analysis of these sources using a single-force inversion formalism suggested that the durations of the slip events were on the order of 50 s (ref. 2). There are certainly differences in flow processes between the WIS and the steeper glaciers of the Northern Hemisphere, so it is not yet clear whether our observations are applicable outside the Antarctic. However, the WIS results reported here show that at least for stick–slip motion of large ice streams, the seismic packets represent the onset and termination of much longer (~25 min) slip episodes. The amplitudes of these signals are largely a function of the rupture velocity and duration of the slip, rather than the total displacement of the ice. Seismic observations can thus detect which glaciers and ice streams show stick–slip behaviour and identify the times and characteristics of the slip events, but are relatively insensitive to the total amount of ice movement.

METHODS SUMMARY

The GPS antennas were clamped to steel poles driven into the snow surface. The 0.1-Hz dual-frequency GPS data were processed relative to a base station installed on nearby stationary ice. Site motion was loosely constrained at 0.05 m every 10 s, which reduces noise without over-smoothing the signal. The precision of the coordinates was assessed during WIS inter-slip time periods or at linearly moving sites and is ~0.01 m and ~0.03 m in the horizontal and vertical coordinates, respectively.

One-dimensional positions were calculated from the resulting GPS horizontal-coordinate time series using vector addition. These positions were filtered using a 600-s low-pass filter to reduce temporally correlated noise, and differentiated to produce velocities (Fig. 2a). The locations and times of slip nucleation were found by picking the first point of the filtered time series that rises above the background noise level and solving for the best-fit origin point and rupture velocity using a least-squares grid-search method. The geographical source regions radiating the second and third surface-wave packets were determined using a grid search over the WIS to find the location best fitting the seismic surface-wave arrival times at QSPA and VNDA as well as the average rupture velocity.

We modelled the seismic waveforms assuming that the source can be represented by a double couple at a very shallow depth (~1 km). We used a reflectivity algorithm and seismic structures appropriate for West Antarctica and East Antarctica for computing the VNDA and, respectively, QSPA synthetics.

Full Methods and any associated references are available in the online version of the paper at www.nature.com/nature.

Received 9 December 2007; accepted 6 April 2008.

1. Ekstrom, G., Nettles, M. & Abers, G. A. Glacial earthquakes. *Science* **302**, 622–624 (2003).
2. Tsai, V. C. & Ekstrom, G. Analysis of glacial earthquakes. *J. Geophys. Res.* **112**, doi:10.1029/2006JF000596 (2007).
3. Ekstrom, G., Nettles, M. & Tsai, V. C. Seasonality and increasing frequency of Greenland glacial earthquakes. *Science* **311**, 1756–1758 (2006).
4. Bindschadler, R. A., King, M. A., Alley, R. B., Anandakrishnan, S. & Padman, L. Tidally controlled stick-slip discharge of a West Antarctic Ice Stream. *Science* **301**, 1087–1089 (2003).

5. Bindschadler, R. A., Vornberger, P. L., King, M. A. & Padman, L. Tidally driven stick-slip motion in the month of Whillans Ice Stream, Antarctica. *Ann. Glaciol.* **36,** 263–272 (2003).
6. Bindschadler, R. A. & Bentley, C. R. On thin ice? *Sci. Am.* **287,** 98–105 (2002).
7. de Angelis, H. & Skvarca, P. Glacier surge after ice shelf collapse. *Science* **299,** 1560–1562 (2003).
8. Scambos, T., Bohlander, J., Shuman, C. & Skvarca, P. Glacier acceleration and thinning after ice shelf collapse in the Larsen B embayment, Antarctica. *Geophys. Res. Lett.* **31,** doi:10.1029/2004GL020670 (2004).
9. Fischer, U. H. & Clarke, G. K. C. Stick-slip sliding behaviour at the base of a glacier. *Ann. Glaciol.* **24,** 390–396 (1997).
10. Aki, K. Generation and propagation of G waves from the Niigata earthquake of June 16, 1964. Part 2. Estimation of earthquake moment, released energy, and stress-strain drop from the G-wave spectrum. *Bull. Earthq. Res. Inst., Tokyo Univ.* **44,** 73–88 (1966).
11. Wiens, D. A., Anandakrishnan, S., Nyblade, A. & Aleqabi, G. Remote detection and monitoring of glacial slip from Whillans Ice Stream using seismic Rayleigh waves recorded by the TAMSEIS array. *Eos* **87,** abstr.–S44A-04 (2006).
12. Joughin, I. *et al.* Continued deceleration of Whillans Ice Stream, West Antarctica. *Geophys. Res. Lett.* **32,** doi:10.1029/2005GL024319 (2005).
13. Bindschadler, R. A., Stephenson, S. N., MacAyeal, D. R. & Shabtaie, S. Ice dynamics at the mouth of Ice Stream B, Antarctica. *J. Geophys. Res.* **92,** 8885–8894 (1987).
14. Alley, R. B. In search of ice-stream sticky spots. *J. Glaciol.* **39,** 447–454 (1993).
15. Peters, M. E., Blankenship, D. D. & Morse, D. L. Analysis techniques for coherent airborne radar sounding: Application to West Antarctic ice streams. *J. Geophys. Res.* **110,** doi:10.1029/2004JB003222 (2005).
16. Das, S. & Aki, K. Fault planes with barriers: A versatile earthquake model. *J. Geophys. Res.* **82,** 5648–5670 (1977).
17. Lay, T. & Kanamori, H. in *Earthquake Prediction: An International Review* (eds Simpson, D. W. & Richards, P. G.) 579–592 (American Geophysical Union, Washington DC, 1981).
18. Anandakrishnan, S., Voigt, D. E., Alley, R. B. & King, M. A. Ice stream D flow speed is strongly modulated by the tide beneath the Ross Ice Shelf. *Geophys. Res. Lett.* **30,** doi:10.1029/2002GL016329 (2003).
19. Russell, D. R. Development of a time-domain, variable-period surface-wave magnitude measurement procedure for application at regional and teleseismic distances. *Bull. Seismol. Soc. Am.* **96,** 665–677 (2006).
20. Beroza, G. C. & Jordan, T. H. Searching for slow and silent earthquakes using free oscillations. *J. Geophys. Res.* **95,** 2485–2510 (1990).
21. Rhie, J. & Romanowicz, B. Excitation of the Earth's continuous free oscillations by atmosphere-ocean-seafloor coupling. *Nature* **431,** 552–556 (2004).
22. Kanamori, H. & Given, J. W. Use of long-period surface waves for rapid determination of earthquake source parameters. *Phys. Earth Planet. Inter.* **27,** 8–31 (1981).
23. Suda, N., Kazunari, K. & Fukao, Y. Earth's background free oscillations. *Science* **279,** 2089–2091 (1998).
24. Horgan, H. J. & Anandakrishnan, S. Static grounding lines and dynamic ice streams: Evidence from the Siple Coast, West Antarctica. *Geophys. Res. Lett.* **33,** doi:10.1029/2006GL027091 (2006).
25. Padman, L., Fricker, H. A., Coleman, R., Howard, S. L. & Erofeeva, S. A new tidal model for the Antarctic ice shelves and seas. *Ann. Glaciol.* **34,** 247–254 (2002).

Supplementary Information is linked to the online version of the paper at www.nature.com/nature.

Acknowledgements GPS receivers for the TIDES project were supplied by the University NAVSTAR Consortium. Seismic data were obtained from the Data Management Center of the Incorporated Research Institutions for Seismology. This research was funded by the Office of Polar Programs, US National Science Foundation. M.A.K. was partially funded by a NERC (UK) research fellowship. We thank R. B. Alley, R. A. Bindschadler, H. Horgan, I. Joughin, L. Peters and D. E. Voigt for planning and carrying out the TIDES field deployment.

Author Contributions D.A.W. found the ice slip signals on the seismic records and carried out the seismic processing and modelling. D.A.W. also filtered the GPS time series and calculated the slip nucleation locations and times from the GPS records. S.A. and J.P.W. carried out the GPS fieldwork and calculated the displacement time series from the three-dimensional GPS data. M.A.K. processed the raw GPS data to obtain the three-dimensional displacement time series. All authors participated in the interpretation of the results and preparing the paper.

Author Information Reprints and permissions information is available at www.nature.com/reprints. Correspondence and requests for materials should be addressed to D.A.W. (doug@wustl.edu).

METHODS

GPS data analysis. The GPS antennas were mounted on poles at a height 1.5–2 m above the surface. Data were logged using Trimble NetRS dual-frequency receivers. The GPS data had a sample rate of 0.1 Hz and were processed relative to a base station installed on nearby stationary ice, giving baselines of length 37–147 km. Base station coordinates were determined in the International Terrestrial Reference Frame 2000 using a Precise Point Positioning approach[26]. Kinematic Precise Point Positioning solutions confirmed that the base station was moving to a negligible degree. When positioning the ice stream sites, data for each baseline were analysed in turn using the Track software[27], solving for three-dimensional WIS site coordinates and tropospheric zenith delay parameters at the full data rate. Carrier phase ambiguities were fixed to integers where possible. GPS satellite positions were adopted from the International GNSS Service final, precise orbit products[28]. In relative positioning over these baseline lengths, ocean tide loading displacements and other unmodelled large-scale loading displacements are reduced to negligible levels. Data were processed in 28-h windows centred on 12:00 UT to reduce day boundary jumps and the coordinate time series were subsequently truncated to cover a single day. Site motion was loosely constrained at 0.05 m every 10 s, which reduces noise without over-smoothing the signal. The precision of the coordinates was assessed during WIS inter-slip time periods or at linearly moving sites and is ~0.01 m and ~0.03 m in the horizontal and vertical coordinates, respectively.

One-dimensional positions were calculated from the resulting GPS horizontal-coordinate time series using vector addition. These positions were filtered using a 600-s low-pass filter to reduce temporally correlated noise, and differentiated to produce velocities (Fig. 2). The nucleation points of the slip events were found by picking the first point of the filtered time series that rises above the background noise level and solving for the best-fit origin point and constant rupture velocity using a grid-search method and a least-squares criterion. The rupture velocity was found to decrease, and the misfit to increase, if more distant sites were included, suggesting that rupture velocity decreases with distance from the origin; therefore, the final locations were determined using only the five GPS receivers nearest the origin point.

Seismic data analysis. The geographical source regions radiating the second and third surface-wave packets were determined by first constraining the average velocities for Love-wave propagation to QSPA and Rayleigh-wave propagation to VNDA using the initial packet, for which the source location is known from GPS measurements (see above). Then we performed a grid search over the WIS to find the location best fitting the seismic surface-wave arrival times as well as the average rupture velocity of the source, starting from the observed nucleation point and using a least-squares criterion.

We modelled the seismic waveforms assuming that the source can be represented by a double couple at a very shallow depth (1 km). Previous studies of long-period surface-wave radiation from glacial sources[2] have used a single-force formalism[29,30]. However, double-couple and horizontal single-force solutions become identical for very shallow sources[31]; thus, either formalism should be valid. In this case some approximation in the modelled signal amplitude may be introduced by the assumption of there being similar shear moduli on both sides of the dislocation, but this approximation should be satisfactory because we do not attempt to make a precise interpretation of the signal amplitude in terms of source properties. The source is assumed to occur in the till layer near the base of the ice stream, but there is very little difference if the source is placed in the ice itself, as the shear moduli of ice and water-saturated till are similar[32].

We used a reflectivity algorithm[33] to compute the synthetics. Because the path from the WIS to VNDA traverses mostly the Ross Sea, for the VNDA synthetics we assumed a crust and mantle structure that was determined from surface waves in the region of the Ross Sea around Ross Island[34]. For the QSPA synthetics we used a seismic structure determined from surface waves in East Antarctica[34] with an appropriate thickness of ice, as the largest portion of the path traverses East Antarctic lithosphere near the South Pole.

26. Zumberge, J. F., Heflin, M. B., Jefferson, D. C., Watkins, M. M. & Webb, F. H. Precise point positioning for the efficient and robust analysis of GPS data from large networks. *J. Geophys. Res.* **102,** 5005–5017 (1997).
27. Chen, G. *GPS Kinematics Positioning for the Airborne Laser Altimetry at Long Valley, California.* PhD thesis, Massachusetts Institute of Technology (1998).
28. Dow, J. M., Neilan, R. E. & Gendt, G. The international GPS service: celebrating the 10th anniversary and looking to the next decade. *Adv. Space Res.* **36,** 320–326 (2005).
29. Eissler, H. K. & Kanamori, H. A single-force model for the 1975 Kalapana, Hawaii, earthquake. *J. Geophys. Res.* **92,** 4827–4836 (1987).
30. Kawakatsu, H. Centroid single force inversion of seismic waves generated by landslides. *J. Geophys. Res.* **94,** 12363–12374 (1989).
31. Dahlen, F. A. Single-force representation of shallow landslide sources. *Bull. Seismol. Soc. Am.* **83,** 130–143 (1993).
32. Anandakrishnan, S. & Winberry, J. P. Antarctic subglacial sedimentary layer thickness from receiver function analysis. *Global Planet. Change* **42,** 167–176 (2004).
33. Kennett, B. L. N. *Seismic Wave Propagation in Stratified Media* (Cambridge Univ. Press, Cambridge, UK, 1983).
34. Lawrence, J. F. *et al.* Rayleigh wave phase velocity analysis of the Ross Sea, Transantarctic Mountains, and East Antarctica from a temporary seismic deployment. *J. Geophys. Res.* **111,** doi:10.1029/2005GL024523 (2006).